(11) (C) **1,319,034**

(21)   453,220

(22)   1984/05/01

(45)   1993/06/15

(52)   75-145

(51) INTL.CL.⁵ H01F-1/053

(19) (CA) **CANADIAN PATENT** (12)

(54) High Energy Product Rare Earth-Iron Magnet Alloys

(72) Croat, John J. , U.S.A.

(73) General Motors Corporation , U.S.A.

(30) (US) U.S.A.   544,728 1983/10/26
    (US) U.S.A.   508,266 1983/06/24

(57) 9 Claims

Canada

C-3515

HIGH ENERGY PRODUCT RARE EARTH-IRON MAGNET ALLOYS

Abstract

Magnetically hard compositions having high values of coercivity, remanence and energy product contain rare earth elements, transition metal elements and boron in suitable proportions. The preferred rare earth elements are neodymium and praseodymium, and the preferred transition metal element is iron. The magnetic alloys have characteristic very finely crystalline microstructures.

C-3515

HIGH ENERGY PRODUCT RARE EARTH-IRON MAGNET ALLOYS

The invention relates to permanent magnet
alloys of rare earth elements, transition metal

5   elements and boron.

Background

United States Patent No. 4,496,395, entitled
"High Coercivity Rare Earth-Iron Magnets", assigned
to the assignee hereof, discloses novel magnetically

10 hard compositions and the method of making them.
More specifically, it relates to alloying mixtures of
one or more transition metals and one or more rare
earth elements. The alloys are quenched from a
molten state at a carefully controlled rate such that

15 they solidify with extremely fine grained crystalline
microstructures as determinable by X-ray diffraction
of powdered samples. The alloys have room temperature
intrinsic magnetic coercivities after saturation
magnetization of at least about 1,000 Oersteds. The

20 preferred transition metal for the magnet alloys is
iron, and the preferred rare earth elements are
praseodymium and neodymium. Among the reasons why
these constituents are preferred are their relative
abundance in nature, low cost and inherently higher

25 magnetic moments.

I have now discovered a new family of
magnets that have markedly improved properties
compared with my earlier discovery. It is an object
of the subject invention to provide novel magnetically

30 hard compositions based on rare earth elements and
iron with extremely fine grained crystal structures
having very high magnetic remanence and energy

1

products and Curie temperatures well above room temperature. Another object is to create a stable, finely crystalline, magnetically hard, rare earth element and iron containing phase in melted and rapidly quenched alloys so that strong permanent magnets can be reliably and economically produced.

A more specific object is to make magnetically hard alloys by melting and rapidly quenching mixtures of one or more rare earth elements, one or more transition metal elements and the element boron. Such alloys exhibit higher intrinsic coercivities and energy products than boron-free alloys. A more specific object is to make such high strength magnet alloys from iron, boron and lower atomic weight rare earth elements, particularly neodymium and praseodymium. Another object is to make these magnetically hard alloys by melt spinning or a comparable rapid solidification process.

Yet another object of the invention is to provide a novel, stable, rare earth-iron-boron, intermetallic, very finely crystalline, magnetic phase. A more particular object is to control the formation of such phase so that the crystallite size appears to be commensurate with optimum single magnetic domain size either by a direct quench or overquench and subsequent heat treatment. Another particular object is to either directly or indirectly create such optimum domain size crystallites in a melt spun or otherwise rapidly quenched RE-Fe-B alloy, particularly a neodymium or praseodymium-iron-boron alloy.

It is a further object to provide a suitable amount of boron in a mixture of low atomic weight rare earth elements and iron to promote the formation

3

of a stable, very finely crystalline, intermetallic
phase having high magnetic remanence and energy product.
Another particular object is to provide the constituent
metallic elements in suitable proportions to form these
5   new intermetallic phases and then process the alloys
to optimize the resultant hard magnetic properties.

Brief Summary

In accordance with a preferred practice of
the invention, an alloy with hard magnetic properties
10   is formed having the basic formula $RE_{1-x}(TM_{1-y}B_y)_x$.

In this formula, RE represents one or more
rare earth elements. The rare earth elements include
scandium and yttrium in Group IIIA of the periodic
table and the elements from atomic number 57 (lanthanum)
15   through 71 (lutetium). The preferred rare earth
elements are the lower atomic weight members of the
lanthanide series, particularly neodymium and praseo-
dymium. However, substantial amounts of certain other
rare earth elements may be mixed with these preferred
20   rare earth elements without destroying or substantially
degrading the permanent magnetic properties.

TM herein is used to symbolize a transition
metal taken from the group consisting of iron or iron
mixed with cobalt, or iron and small amounts of such
25   other metals as nickel, chromium or manganese. Iron
is necessary to form the new boron-containing magnetic
phase and is also the preferred transition metal
because of its relatively high magnetic remanence and
low cost. A substantial amount of cobalt may be
30   mixed with iron without adverse effect on magnetic
properties. The inclusion of nickel, chromium and
manganese in amounts greater than about 10 percent
has generally been found to have a deleterious effect
on the permanent magnetic properties of the subject
35   Nd-Fe-B alloys.

The most preferred alloys contain the rare
earth elements Nd and/or Pr and the transition metal
element, Fe. The superior properties of these light
rare earth-iron combinations are due, at least in

5 part, to ferromagnetic coupling between the light
rare earth elements and Fe. That is, in optimum
alloys the orbital magnetic moments ($\vec{L}$) of the rare
earths align in the same parallel direction as the
spin moments of the iron ($\vec{S}$) so that the total moment

10 ($\vec{J}$) equals $\vec{L}$ + $\vec{S}$. For the heavy rare earth elements
such as Er, Tb and Ho, the magnetic coupling is
antiferromagnetic and the orbital magnetic moments of
the rare earths are antiparallel to the iron spin
moment so that the total moment $\vec{J} = \vec{L} - \vec{S}$. The total

15 magnetic moment of the ferromagnetically coupled
light rare earth-iron alloys is, therefore, greater
than that of antiferromagnetically coupled heavy rare
earth-iron alloys. The rare earth element, samarium,
may couple ferro or antiferromagnetically with iron,

20 behaving therefore as both a light and a heavy rare
earth element within the context of this invention.

B is the atomic symbol for the element
boron. X is the combined atomic fraction of
transition metal and boron present in a said

25 composition and generally $0.5 \lesssim x \lesssim 0.9$, and
preferably $0.8 \lesssim x \lesssim 0.9$. Y is the atomic fraction
of boron present in the composition based on the
amount of boron and transition metal present. An
acceptable range for y is $0.05 \lesssim y \lesssim 0.10$, the

30 preferred range being $0.05 \lesssim y \lesssim 0.07$. B should not
be present as more than about 10 atomic percent of
the total composition, and preferably less than 7
percent. The incorporation of only a small amount of
boron in alloys having suitable finely crystalline

35 microstructures was found to substantially increase

5

the coercivity of RE-Fe alloys at temperatures up to 200°C or greater, particularly those alloys having high iron concentrations. In fact, the alloy $Nd_{0.2}(Fe_{0.95}B_{0.05})_{0.8}$ exhibited an intrinsic

5   magnetic room temperature coercivity exceeding about 20 kiloOersteds, substantially comparable to the hard magnetic characteristics of much more expensive $SmCo_5$ magnets. The boron inclusion also substantially improved the energy product of the alloy and

10   increased its Curie temperature.

        Permanent magnet alloys in accordance with the invention were made by mixing suitable weight portions of elemental forms of the rare earths, transition metals and boron. The mixtures were arc

15   melted to form alloy ingots. The alloy was in turn remelted in a quartz crucible and expressed through a small nozzle onto a rotating chill surface. This produced thin ribbons of alloy. The process is generally referred to in the art as "melt spinning"

20   and is also described in United States Patent No. 4,496,395. In melt spinning, the quench rate of the melt spun material can be varied by changing the linear speed of the quench surface. By selection of suitable speed ranges I obtained products that

25   exhibited high intrinsic magnetic coercivities and remanence as quenched. Furthermore, I found that products with such properties could be produced either as directly quenched from the melt, or as overquenched and annealed as will be described

30   hereinafter.

        In each case where good magnetic properties were obtained, the magnetic material comprised very small crystallites (about 20 to 400 nanometers average diameter) apparently sized near the optimum

35   single magnetic domain size or smaller. The fairly

6

uniform shape of the crystallites as exhibited by
scanning electron microscopy suggest a crystal
structure that is fairly uniform in all directions
such as a tetragonal or cubic structure.

5   Mathematical modeling based on neutron diffraction
data strongly suggests a tetragonal crystal structure
where a = 8.8 angstroms and c = 12.2 angstroms. The
nominal composition of the magnetic phase is believed
to be $RE_2Fe_{14}B_1$ (e.g. $RE_{.27}Fe_{.72}B_{.01}$ approximate

10   atomic weight fraction; $RE_{.12}Fe_{.82}B_{.06}$ approximate
atomic fractions), where RE is neodymium and/or
praseodymium. As will be substantiated hereinafter,
this crystal phase is not destroyed by substituting
limited amounts of other rare earths and transition

15   metals for the preferred constituent elements.
Alloys of such structure constitute a heretofore
unknown magnetic phase.

        The inclusion of boron in suitable amounts
to mixtures of rare earth elements and iron was found

20   to promote the formation of a stable, hard magnetic
phase over a fairly broad range of quench rates.
The magnetic remanence and energy product of all
melt-spun, magnetically hard, boron-containing,
RE-iron alloys were improved with respect to

25   boron-free compositions. The Curie temperatures of
the alloys were substantially elevated. My invention
will be better understood in view of the following
detailed description.

Detailed Description

30   Figure 1 is a plot of room temperature
intrinsic coercivity for magnetized melt spun
$Nd_{0.4}(Fe_{1-y}B_y)_{0.6}$ alloys as a function of the
linear speed (V_s) of the quench surface.

35

Figure 2 is a plot of room temperature intrinsic coercivity for magnetized melt spun $Nd_{0.25}(Fe_{1-y}B_y)_{0.75}$ alloys versus the linear speed of the quench surface.

Figure 3 is a plot of room temperature intrinsic coercivity for magnetized melt spun $Nd_{0.15}(Fe_{1-y}B_y)_{0.85}$ alloys as a function of the linear speed (V_s) of the quench surface.

Figure 4 is a plot of room temperature intrinsic coercivity for magnetized melt spun $Nd_{1-x}(Fe_{0.95}B_{0.05})_x$ alloys as a function of the linear speed of the quench surface.

Figure 5 is a plot of remanent magnetization B_r of melt spun $Nd_{1-x}(Fe_{0.95}B_{0.05})_x$ alloys at room temperature as a function the linear speed of the quench surface.

Figure 6 shows demagnetization curves for melt spun $Nd_{0.25}(Fe_{0.95}B_{0.05})_{0.75}$ as a function of the linear speed of the quench surface.

Figure 7 shows demagnetization curves for melt spun $Nd_{0.2}(Fe_{0.96}B_{0.04})_{0.8}$ alloy for initial magnetizing fields of 19 kOe and 45 kOe.

Figure 8 shows demagnetization curves for melt spun $Nd_{0.25}(Fe_{1-y}B_y)_{0.75}$ alloys.

Figure 9 is a plot of room temperature intrinsic coercivity for magnetized $Pr_{0.4}Fe_{0.6}$ and $Pr_{0.4}(Fe_{0.95}B_{0.05})_{0.6}$ alloys as a function of the linear speed of the quench surface.

Figure 10 shows demagnetization curves for melt spun $Nd_{0.15}(Fe_{1-y}B_y)_{0.85}$ alloys.

Figure 11 shows a plot of energy product, magnetic remanence and magnetic coercivity for $Nd_{1-x}(Fe_{0.95}B_{0.05})_x$ as a function of neodymium

content, and Figure 12 shows intrinsic coercivities of $Nd_{1-x}(Fe_{0.95}B_{0.05})_x$ alloy as a function of neodymium content.

Figure 13 is a scanning electron micrograph of the fracture surface of a melt spun ribbon of $Nd_{0.135}(Fe_{0.946}B_{0.054})_{0.865}$ alloy as quenched, the micrographs being taken at the free surface, the interior and the quench surface of the ribbon.

Figure 14 shows demagnetization curves (M versus H and B versus H) for the melt spun $Nd_{0.135}(Fe_{0.946}B_{0.054})_{0.865}$ alloy of Figure 13.

Figure 15 shows demagnetization curves for melt spun $Nd_{1-x}(Fe_{0.95}B_{0.05})_x$ alloys.

Figure 16 shows demagnetization curves for melt spun $Nd_{0.33}(Fe_{0.95}B_{0.05})_{0.67}$ at several different temperatures between 295°K and 450°K.

Figure 17 shows demagnetization curves of melt spun $Nd_{0.15}(Fe_{0.95}B_{0.05})_{0.85}$ at several different temperatures between 295°K and 450°K.

Figure 18 plots normalized log values of intrinsic coercivity for three neodymium-iron-boron alloys as a function of temperature.

Figure 19 is a plot showing the temperature dependence of magnetic remanence for several neodymium-iron-boron alloys.

Figure 20 plots the temperature dependence of magnetization for melt spun $Nd_{0.25}(Fe_{1-y}B_y)_{0.75}$ at several different boron additive levels.

Figure 21 plots the magnetization of several melt spun $Nd_{1-x}(Fe_{0.95}B_{0.05})_x$ alloys as a function of temperature.

Figure 22 shows representative X-ray spectra for melt spun $Nd_{0.15}(Fe_{1-y}B_y)_{0.85}$ alloy for values of two theta between about 20 and 65 degrees.

9

Figure 23 shows X-ray spectra of melt spun $Nd_{0.25}(Fe_{0.95}B_{0.05})_{0.75}$ taken of material located on the quench surface of a ribbon of the alloy and of a sample of material from the free surface remote from

5   the quench surface.

Figure 24 shows differential scanning calorimetry tracings for $Nd_{0.25}(Fe_{1-y}B_y)_{0.75}$ alloys taken at a heating rate of 80°K per minute.

Figure 25 shows differential scanning

10   calorimetry traces for $Nd_{0.15}(Fe_{0.85})$, $Nd_{0.15}(Fe_{0.95}B_{0.05})_{0.85}$ and $Nd_{0.15}(Fe_{0.91}B_{0.09})_{0.85}$ taken at a heating rate of 80°K per minute for melt-spinning quench speeds of $V_s = 30$ and 15 m/s.

Figure 26 shows typical demagnetization

15   curves for several permanent magnet materials and values of maximum magnetic energy products therefor.

Figure 27 shows the effect of adding boron to $Nd_{1-x}(Fe_{1-y}B_y)_x$ alloys on Curie temperature.

Figure 28 is a plot showing the relative

20   coercivities of samples of $Nd_{0.15}(Fe_{0.95}B_{0.05})_{0.85}$ melt spun at quench wheel speeds of 30 and 15 meters per second and thereafter annealed at about 850°K for 30 minutes.

Figure 29 is a demagnetization curve for

25   $Nd_{0.14}(Fe_{0.95}B_{0.05})_{0.86}$ originally melt spun and quenched at $V_s = 30$ m/s and then taken to a maximum anneal temperature of Ta = 950°K at a ramp rate of 160°K per minute, held for 0, 5, 10 and 30 minutes.

Figure 30 is a comparison of the demagnet-

30   ization curves for $Nd_{0.14}(Fe_{0.95}B_{0.05})_{0.86}$ alloy melt spun and quenched at wheel speeds of $V_s = 27.5$ and 30 m/s and annealed at ramp rates of 160 and 40°K per minute.

35

10

Figure 31 is a plot of maximum energy product as a function of the linear speed of the quench surface for $Nd_{0.14}(Fe_{0.95}B_{0.05})_{0.86}$ alloy. The open circles form the curve for the alloy as quenched, while the open squares, triangles and closed circles represent material melt spun at the indicated V_s value and later annealed at a ramp rate of 160°K per minute to maximum temperatures of 1000, 975 and 950°K.

Figure 32 is a demagnetization curve for $Nd_{0.135}(Fe_{0.935}B_{0.065})_{0.865}$ alloy at several linear quench surface speeds also indicating maximum energy product for a particular V_s.

Figure 33 shows X-ray powder diffraction patterns of $Nd_{0.135}(Fe_{0.935}B_{0.065})_{0.865}$ ingot and alloy melt spun and quenched at several different quench surface speeds (V_s).

Figure 34 shows differential scanning calorimetry tracings for $Nd_{0.135}(Fe_{0.946}B_{0.054})_{0.865}$ alloy taken at a heating rate of 160°K per minute for alloys quenched at V_s = 19, 20.5 and 35 m/s.

Figure 35 is a demagnetization curve for $Nd_{0.135}(Fe_{0.946}B_{0.054})_{0.865}$ alloy originally quenched at a linear quench surface rate of V_s = 20.5 m/s and then annealed at heating and cooling ramp rates of 160°K per minute to maximum temperatures of 950, 975 and 1000°K indicating the maximum energy product for each.

Figure 36 is a curve like that of Figure 35 except that V_s = 35 m/s.

Figure 37 is a panel of three scanning electron micrographs taken along the fracture surface of a melt spun ribbon of $Nd_{0.14}(Fe_{0.95}B_{0.05})_{0.86}$ alloy where the linear speed of the quench surface $V_s =$

5   30 m/s. The SEM's are representative of the microstructure near the free surface, the center and the quench surface of the ribbon.

Figure 38 is a panel of three scanning electron micrographs taken along the fracture surface

10   of a melt spun ribbon of $Nd_{0.14}(Fe_{0.95}B_{0.05})_{0.86}$ alloy originally quenched at a linear quench surface speed of $V_s = 30$ m/s and then annealed at a maximum temperature of 950°K at a heating and cooling ramp rate of 160°K per minute, the SEM's being taken near

15   the free surface, the center, and the quench surface of the ribbon.

Figure 39 is a demagnetization curve for $Nd_{0.135}(Fe_{0.946}B_{0.054})_{0.865}$ alloy originally quenched at linear quench surface rates of $V_s =$

20   29, 20.5 and 35 m/s, annealed at 950°K maximum at a heating and cooling ramp rate of 160°K per minute.

Figure 40 is a demagnetization curve for $Pr_{0.135}(Fe_{0.935}B_{0.065})_{0.86}$ alloy melt spun at a linear quench surface speed of $V_s = 30$ m/s and

25   then annealed at a ramp rate of 160°K per minute to maximum temperatures of 900, 925 and 975°K.

Figure 41 is a plot of $RE_{0.135}(Fe_{0.935}B_{0.065})_{0.865}$ melt spun and quenched at a linear quench surface speed of $V_s = 30$ and

30   then annealed to a maximum temperature of 950°K at a heating and cooling ramp rate of 160°K per minute where RE is praseodymium, neodymium, samarium, lanthanum, cerium, terbium and dysprosium.

35

12

Figure 42 is a demagnetization curve for $(Nd_{0.8}RE_{0.2})_{0.135}(Fe_{0.935}B_{0.065})_{0.865}$ alloy melt spun and quenched at a linear quench surface speed V_s = 30 m/s and then annealed at a heating and cooling

5   ramp rate of 160°K per minute to a maximum temperature of 950°K.

Figure 43 is a demagnetization curve for $Nd_{0.135}(TM_{0.935}B_{0.065})_{0.865}$ alloys originally melt spun at a quench speed of V_s = 30 m/s

10   annealed at a ramp rate of 160°K per minute to a maximum temperature of 950°K, where TM is iron, cobalt and nickel.

Figure 44 shows demagnetization curves for $Nd_{0.135}(Fe_{0.841}TM_{0.094}B_{0.065})_{0.865}$ alloy originally

15   melt spun at a quench surface speed of V_s = 30 m/s annealed at a heating and cooling ramp rate of 160°K per minute to a maximum temperature of 950°K, where TM is cobalt, nickel, chromium, manganese and copper.

Figure 45 is a demagnetization curve for

20   $Nd_{0.135}(Fe_{0.784}TM_{0.187}B_{0.065})_{0.865}$ alloys originally melt spun at a quench surface rate of V_s = 30 m/s and then annealed at a heating and cooling ramp rate of 160°K per minute to a maximum temperature of 950°K, where TM is cobalt, nickel, chromium and

25   manganese.

Figure 46 shows a neutron diffraction pattern for melt spun $Nd_{.135}(Fe_{0.945}B_{0.055})_{0.865}$ ribbon taken at 673°K, a calculated pattern for a tetrahedral crystal of nominal atomic formula

30   $Nd_2Fe_{14}B$ and a plot which is the differential of the observed and calculated patterns.

35

13

Figure 47 shows the atomic arrangement of atoms in four cells in the basal plane ($z = 0$) of the $Nd_2Fe_{14}B$ crystal structure as determined by neutron diffraction data.

Figure 48 shows the projection of atoms nearest the planes defined by $z = 0.16$ and 0.84 (based on the c axis).

Figure 49 shows the arrangement of atoms in the $z = 0.25$ and 0.75 planes.

Figure 50 shows the projection of atoms nearest the planes defined by $Z = 0.34$ and 0.66.

Figure 51 shows the arrangement of atoms in the $z = 0.5$ plane.

Figure 52 shows the complete unit cell of the tetrahedral $Nd_2Fe_{14}B$ crystal where the length of the c axis has been exaggerated to show the puckering of the hexagonal iron meshes.

This invention relates to making improved magnetically hard rare earth-transition metal compositions incorporating small amounts of the element boron. The invention also relates to quenching molten mixtures of the constituent elements at a rate between that which yields a magnetically soft amorphous material and a magnetically soft crystalline material.

Herein, H refers to the strength of an applied magnetic field; H_{ci} is the intrinsic coercive force or reverse field required to bring a magnetized sample having magnetization M back to zero magnetization; M is the magnetization of a sample in electromagnetic units; M_s is the saturation magnetization or the maximum magnetization that can be induced in a sample by an applied magnetic field; B is the magnetic induction or magnetic flux density of a sample where $B = H + 4\pi M$ (emu), where B, M and H are in units of Gauss or Oersteds; B_r is

13

14

the remanent magnetic induction; BH is the energy
product; and T is temperature in degrees Kelvin
unless otherwise indicated. The terms "hard magnet"
and "magnetically hard alloy" herein refer to compo-
5   sitions having intrinsic coercivities of at least
about 1,000 Oersteds.

Melt Spinning

         Melt spinning is a well known process
which has been used to make "metglasses" from high
10   alloy steels. As it relates to this invention, melt
spinning entails mixing suitable weight portions of
the constituent elements and melting them together to
form an alloy of a desired composition. Arc melting
is a preferred technique for experimental purposes
15   because it prevents any contamination of the alloys
from the heating vessel.

         In the following examples, alloy ingots
were broken into chunks small enough to fit inside a
spin melting tube (crucible or tundish) made of
20   quartz. Ceramic, or other suitable refractory
materials could be used. Each tube had a small
orifice in its bottom through which an alloy could be
ejected. The top of the tube was sealed and provided
with means for containing pressurized gas in the tube
25   above a molten alloy. A heating coil was disposed
around the portion of the tube containing the alloy
to be melt spun. When the coil was activated, the
chunks of alloy within the tube melted and formed a
fluid mass.

30   An inert gas was introduced into the space
above the molten alloy at a constant positive
pressure to eject it through the small orifice at a
constant rate. The orifice was located only a short
distance from a chill surface on which the molten
35   metal was rapidly cooled and solidified into ribbon

14

1319034

form. The surface was the outer perimeter of a
rotating copper disc plated with chromium although
other chill surfaces and materials such as molybdenum
having high thermal conductivity may also be
5   acceptable.

The disc was rotated at a constant speed so
that the relative velocity between the ejected alloy
and the chill surface was substantially constant.
However, the rate at which a quench surface moves may
10   be varied throughout a run to compensate for such
factors as the heating of the quench surface varied
alloy melt temperature or to create a desired micro-
structure in the ribbon.

Herein, the disc speed (V_s) is the speed
15   in meters per second of a point on the chill surface
of the melt spinner's quench disc as it rotates at a
constant rotational velocity. Because the chill disc
is much more massive than the alloy ribbon, it acts
as an infinitely thick heat sink for the metal that
20   solidifies on it. The disc may be cooled by any
suitable means to prevent heat build-up during long
runs. The terms "melt-spinning" or "melt-spun" as
used herein refer to the process described above as
well as any like process which achieves a like
25   result.

The principal limiting factor for the rate
of chill of a ribbon of alloy on the relatively
cooler disc surface is its thickness. If the ribbon
is too thick, the metal most remote from the chill
30   surface will cool too slowly and crystallize in a
magnetically soft state. If the alloy cools very
quickly, the ribbon will have a microstructure that
is somewhere between almost completely amorphous and
very, very finely crystalline.

35

1319034

16

Overquenched melt spun ribbons have low
intrinsic magnetic coercivity, generally less than a
few hundred Oersteds. If they are amorphous, i.e.
completely glassy, they cannot be later annealed to
5   achieve magnetic properties comparable to an alloy
directly quenched at the optimum rate. However, if
an alloy is cooled at a slightly slower rate than
that which produces a glass, an incipient micro-
crystalline structure seems to develop. The slightly
10   overquenched alloy has low coercivity as formed but
has the capacity to develop a near optimum micro-
crystalline hard magnetic phase. That is, a control-
led rapid anneal of a partially overquenched alloy
can promote the development of a finely crystalline
15   hard magnetic phase. This phase appears to be the
same as that present in the best directly quenched,
boron-containing alloy ribbon.

In all of the following examples, a melt
spinning apparatus of the type described above was
20   used to make ribbons of the novel magnetic composi-
tions. The quartz tube for Examples 1, 2, 4-9, 12-20
and 23-24 was about 100 mm long and 12.7 mm in
diameter. About 4 grams of alloy chunks were added
to the tube for each run. The ejection orifice was
25   round and about 500 microns in diameter, and an argon
ejection pressure of about 5 psi was used. For the
remaining examples, the quartz tube was about 127 mm
long and about 25 mm in diameter. About 25-40 grams
of alloy chunks were added to the tube for each run.
30   The ejection orifice was round and about 675 microns
in diameter. An argon ejection pressure of about 3.0
psi was used. In each case, the orifice was located
about 1/8 to 1/4 inches from the chill surface of the
cooling disc. The disc was initially at room tempera-
35   ture and was not externally cooled. The resultant

16

17

melt spun ribbons were about 30-50 microns thick and
about 1.5 millimeters wide.

The critical element of the melt-spinning
process is the controlled quenching of the molten
5   alloy to produce the desired very fine crystalline
microstructure. While melt spinning is a preferred
method of making the subject boron enhanced RE-TM
magnet materials, other comparable methods may be
employed.

10   X-ray data supports the hypothesis that the
hard magnetic phase is, in fact, very finely crystal-
line. Scanning electron microscopy results indicate
that the optimum average crystallite size is between
about 20 and 400 nanometers. I believe that such
15   small crystallite size is nearly commensurate with
optimum single domain size for the subject RE-Fe-B
alloys.

Compositions

The magnetic compositions of this invention
20   are formed from molten homogeneous mixtures of
certain rare earth elements, transition metal
elements and boron.

The rare earth elements include scandium
and yttrium in group IIIA of the period table as well
25   as the lanthanide series elements from atomic No. 57
(lanthanum) through atomic No. 71 (lutetium). In
order to achieve the desired high magnetic coercivities
for the subject magnet compositions, I believe that
the f-orbital of the preferred rare earth constituent
30   elements or alloys should not be empty, full or half
full. That is, there should not be zero, seven or
fourteen electrons in the f-orbital of the alloyed
rare earth constituent.

35

18

The preferred rare earth elements for use
in this invention are two lower atomic weight members
of the lanthanide series, neodymium and praseodymium.
These elements are also commonly referred to as light
rare earth elements. Nd and Pr are among the most
abundant, least expensive, and have the highest
magnetic moments of the light rare earths. The
elements Nd and Pr also couple ferromagnetically with
iron (total moment, $\vec{J} = \vec{L} + \vec{S}$).

It is usually possible to substitute rare
earth elements for one another in the crystal lattice
of an alloy. For example, if the atomic radius of a
rare earth element is critical to the behavior and
micrographic structure of an alloy in which it is
mixed with a transition metal, by the substitution
of two different rare earth elements with a suitable
average atomic radius (e.g., one with a greater atomic
radius and one with a smaller radius), one may produce
an alloy with like crystallographic structure.

Therefore, it may be possible to substitute
controlled amounts of other rare earth elements for
Pr and Nd in our alloys. However, the heavier rare
earth elements such as terbium, holmium, dysprosium,
erbium and thulium couple anti-ferromagnetically with
iron. Therefore, these heavy rare earth-containing
iron alloys would not be expected to produce permanent
magnets as strong as Nd-Fe and Pr-Fe alloys.

The elements iron, nickel, cobalt, chromium,
copper and manganese are transition metals. In the
practice of this invention, iron is a necessary and
preferred constituent. Moreover, it is·relatively
abundant in nature, inexpensive and inherently high
in magnetic remanence. Cobalt may be substituted for
a portion of this iron. While small amounts of the

other transition metals may not interfere severely with the permanent magnetic properties of the subject alloys, they have not been found to augment the permanent magnetic properties either.

5   Boron was used in elemental form in all cases as were the rare earth and transition metal elements. However, alloyed forms of boron and the other elements may be equally suited. Small amounts of other elements may be present so long as they do
10   not significantly deteriorate the magnetic properties of the compositions.

The relative amounts of RE, TM and B alloyed together are expressed herein in terms of atomic fractions or percents. A distinction is made
15   herein between atomic fractions and atomic weight fractions. For example, one atomic weight unit of the composition having the atomic fraction formula $Nd_{0.4}(Fe_{0.95}B_{0.05})_{0.6}$ would comprise by weight:

20   0.4 x atomic wt. Nd = 0.4 x 144.24 = 57.696 g Nd
0.6 x 0.95 x atomic wt. Fe = 0.57 x 55.85 = 31.835 g Fe
0.6 x 0.05 x atomic wt. B = 0.03 x 10.81 = <u>0.324</u> g B
89.855 g Total

which expressed as weight fractions or weight percents
25   of the constituents is:

	wt. fraction	wt. percent
Nd	57.696/89.855 = 0.642	64.2
Fe	31.835/89.855 = 0.354	35.4
B	0.324/89.855 = 0.004	0.4

30   The preferred compositional range for the subject hard magnet alloys of this invention is about 10 to 20 atomic percent rare earth elements with the balance being transition metal elements and a small amount (less than about 10 and preferably less than
35

20

about 7 atomic percent total) boron. Higher percent-
ages of the rare earth elements are possible but may
adversely affect the magnetic energy product. Small
amounts of other elements may be present so long as
5   they do not materially adversely affect the practice
of the invention. My invention will be better
understood in view of the following examples.

Example 1

Referring to Figure 1, alloys of neodymium
10 and iron were made by mixing substantially pure
commercially available forms of the elements in
suitable weight proportions. The mixtures were arc
melted to form alloy ingots. The amount of neodymium
was maintained in each alloy at an atomic fraction of
15 0.4. The iron and boron constituents together made
up an atomic fraction of 0.6. The atomic fraction of
boron, based on the amount of iron present was varied
from 0.01 to 0.03. Each of the alloys was melt spun
by the method described above. The quench rate for
20 each alloy was changed by varying the surface velocity
of the quench wheel. About four grams of ribbon were
made for each sample.

The intrinsic coercivity of each of the
alloys for this and the other examples was determined
25 as follows. The alloy ribbon was first pulverized to
powder with a roller on a hard surface. Approximately
100 mg of powder was compacted in a standard cylindri-
cal sample holder for the magnetometer. The sample
was then magnetized in a pulsed magnetic field of
30 approximately 45 kiloOersteds. This field is not
believed to be strong enough to reach magnetic
saturation (M_s) of the subject alloys but was the
strongest available for my work. The intrinsic
coercivity measurements were made on a Princeton
35 Applied Research vibrating sample magnetometer with

21

a maximum operating field of 19 kOe. Magnetization values were normalized to the density of the arc melted magnet material.

It can be seen from Figure 1 that the intrinsic coercivity (H_{ci}) is dependent both on quench rate (a function of V_s) and boron content. The highest overall intrinsic coercivities were achieved for the neodymium iron alloy containing the most boron (3 percent) based on iron. Lesser percentages of boron improved the intrinsic coercivity of the composition over boron-free alloy. The optimum substrate velocity appeared to be about 7.5 meters per second for the small quartz tube with the 500 micron ejection orifice and an ejection pressure of about 5 psi. Intrinsic coercivities were lower for wheel speeds below 5 meters per second and above 15 meters per second.

Example 2

Figure 2 is a plot of intrinsic magnetic coercivity versus substrate quench speed for alloys of neodymium and iron where neodymium comprises 25 atomic percent of the alloy. The samples were made and tested as in Example 1. Clearly, the inclusion of boron in amounts of three and five atomic percent based on iron content greatly improved the intrinsic room temperature coercivity for these alloys. Without boron, this high iron content alloy does not show very high intrinsic coercivity (2.3 kOe maximum). It appears that the inclusion of even a small amount of boron can create high intrinsic magnetic coercivity in certain alloys where it would otherwise not be present. The $Nd_{0.25}(Fe_{0.95}B_{0.05})_{0.75}$ alloy (3.75 atomic percent B) achieved an H_{ci} of 19.7 kOe comparable, e.g., to the intrinsic coercivities of rare earth-cobalt magnets.

22

Example 3

Figure 3 is a plot of intrinsic room
temperature coercivity as a function of quench
velocity for melt spun ribbons of $Nd_{0.15}(Fe_{1-y}B_y)_{0.85}$

5   alloy, wherein the fraction of boron with respect to
iron was 0.03, 0.05, 0.07 and 0.09. In this example,
the alloy was melt spun from the larger quartz tube
having an orifice diameter of about 675 microns at an
ejection pressure of about 3 psi argon. The maximum

10   coercivity was achieved for y = 0.07 at a quench
surface velocity of about 17.5 meters per second.
The maximum intrinsic coercivity for y = 0.05 and
0.09 were both lower than y = 0.07. The 0.09 also
had a narrower window of quench rates over which the

15   high coercivity magnetic phase formed. The inclusion
of 0.03 boron increased the intrinsic coercivity of
the alloy as compared to that with no boron, but the
highest value of intrinsic coercivity was substan-
tially lower than that for higher boron content alloys.

20   ### Example 4

Figure 4 is a plot of intrinsic room
temperature coercivity as a function of quench
velocity for melt spun alloy ribbons of neodymium,
iron and boron where the Nd content was varied from

25   10 to 30 atomic percent and the ratio of iron to
boron is held constant at 0.95 to 0.05. The maximum
coercivity achieved for the ten atomic weight percent
neodymium alloy was only about 6 kiloOersteds. For
15 atomic percent neodymium the maximum intrinsic

30   coercivity achieved was about 17 kiloOersteds. For
all other neodymium contents, however, the maximum
intrinsic coercivity was at least about 20 kilo-
Oersteds. The optimum quench velocity for these
alloys appeared to be in the 10 to 15 meter per

35   second range.

Example 5

Figure 5 is a plot of remanent magnetization (B_r) measured at room temperature for melt spun neodymium iron alloys as a function of substrate quench speed. For the high iron content alloys there is clearly a critical substrate quench velocity beyond which the magnetic remanence of the material falls off rapidly. At substrate quench speeds less than 20 meters per second, all of the neodymium alloys showed remanent magnetization values of at least about 4 kiloGauss. Increasing the Fe concentration results in an appreciable increase in remanent magnetization from a maximum of 4.6 kG at X = 0.67 to 8.0 kG for X = 0.9. A carefully controlled, rapid anneal of overquenched ribbon $(V_s > 20$ m/s, e.g.) can be affected as will be described hereinafter to induce coercivity and remanence commensurate with optimally quenched alloy.

Example 6

Figure 6 is a demagnetization curve for melt spun $Nd_{0.25}(Fe_{0.95}B_{0.05})_{0.75}$ for several different substrate chill velocities. The relatively square hysteresis loop characterized by the relatively flat demagnetization curves in the second quadrant for $V_s = 7.5$ and $V_s = 10$ meters per second is desirable for many hard magnet applications as it results in higher energy products.

Example 7

Figure 7 shows demagnetization curves for melt spun $Nd_{0.2}(Fe_{0.96}B_{0.04})_{0.8}$ alloy as a function of the initial magnetizing field. The curve is substantially lower for the 19 kiloOersted magnetizing field than the 45 kiloOersted field. As noted

in Example 1, I believe that higher remanent magnet-
ization and H_{ci} could be achieved for the subject
RE-Fe-B compositions given a stronger magnetizing
field strong enough to induce magnetic saturation.

5
Example 8

Figure 8 shows demagnetization curves for
melt-spun 25 atomic percent neodymium iron alloys.
The addition of 0.03 and 0.05 atomic fractions boron
(based on iron content) served to substantially

10 flatten and extend the demagnetization curves for
this alloy indicating higher energy products. Higher
boron levels than those shown in Figure 7, e.g., y =
0.07, result in small additional increases in coer-
civity but remanent magnetization drops, resulting in

15 lowered energy product.

Generally, not much benefit in intrinsic
coercivity is gained and a loss of energy product may
occur by adding too much boron (based on the total
composition) to a melt-spun rare earth-iron alloys.

20 Excess boron also seems to narrow the window of quench
rates over which the desired magnetic phase forms
directly (See Figure 3, e.g.). Experimental evidence
indicates that a concentration of boron above about
5-6 total atomic percent exceeds the boron concentra-

25 tion of the subject equilibrium magnetic RE-Fe-B
intermetallic phase upon which the hard magnetic
properties of these materials are based. While
excess boron will not destroy the magnetic phase at
concentrations up to and even exceeding 10 atomic

30 percent, boron concentrations over about 6 atomic
percent do dilute the magnetic properties of the
alloys. The inclusion of boron in an amount of about
5-6 percent or less, however, stabilizes the formation
of a crystalline intermetallic magnetic phase which

35

forms into a very finely crystalline, magnetically
hard microstructure during the quench. Excess boron,
above 5-6 atomic percent, appears to promote the
formation of magnetically soft Fe-B glasses.

Example 9

Figure 9 shows the intrinsic room tempera-
ture coercivity for $Pr_{0.4}Fe_{0.6}$ and
$Pr_{0.4}(Fe_{0.95}B_{0.05})_{0.6}$. The addition of a
small amount of boron, here three percent of the
total composition was found to improve the intrinsic
coercivity of praseodymium-iron compounds from
roughly 6.0 to over 16 kOe at quench velocities of
about 7.5 meters per second. While I have exten-
sively examined neodymium-iron systems, other rare
earth and transition metal alloys containing boron
and processed in accordance with the subject invention
will exhibit permanent magnetic properties as will be
described by example hereinafter.

Example 10

Figures 11 and 12 show the properties of
$Nd_{1-x}(Fe_{0.95}B_{0.05})_x$ alloys. The samples were
ejected from the 675 micron capillary onto a quench
wheel moving at the near optimum speed of $V_s = 15$
m/s. Figure 11 shows the energy product (BH), the
magnetic remance B_r and the inductive coercivity
H_c for the several neodymium contents. The remanence,
coercivity and magnetic energy product all peak at an
X (the total atomic fraction of Fe and B) approximately
equal to 0.86. An energy product of 14.1 MG·Oe was
achieved which is nearly commensurate with the energy
product of oriented samarium-cobalt magnets. Figure
12 shows intrinsic coercivity H_{ci}. Maximum H_{ci}
was achieved at about X = 0.75.

26

Figure 13 is a scanning electron micrograph of the transverse fracture surface of a ribbon sample of the 14.1 megaGauss Oersted direct quenched alloy. The micrographs were taken near the quench surface,
5   i.e., that surface which impinges the quench wheel in the melt-spinning process; at the center of the ribbon cross section; and at the free surface, i.e. that surface farthest from the quench wheel.

It has been found that those magnetic
10   materials exhibiting substantially uniform crystal-lite size across the thickness of the ribbon tend to exhibit better permanent magnetic properties than those showing substantial variation in crystallite size throughout the ribbon thickness. The directly
15   quenched material of Figure 13 appears to consist of fine crystallites which range in size from approximately 20 to 50 nanometers. This crystallite size is probably close optimum single magnetic domain size.

Figure 14 shows the demagnetization behavior
20   for the 14.1 megaGauss Oersted directly quenched magnet material. The relatively high remanence of about 8.2 kG contributes substantially to the high energy product (B x H).

Example 11

25   Figure 15 shows the effect of varying the neodymium content $Nd_{1-x}(Fe_{0.95}B_{0.05})_x$ alloys on the second quadrant demagnetization curve. The samples were ejected from the 675 micron capillary at a near optimum quench wheel speed of $V_s = 15$ m/s. For
30   neodymium contents of less than about 10 percent, the inductive coercivity H is less than about 7 kilo-Oersteds. The highest remanence is achieved for neodymium contents of approximately 15 to 13.4 atomic percent. Higher neodymium contents, X = 0.8 and X =
35   0.75 have a tendency to reduce the magnetic remanence

but increase the intrinsic coercivity of directly
quenched alloy. From this information, it has been
hypothesized that the near optimum composition for
neodymium-iron-boron alloys contain approximately 14
5 percent neodymium. However, there may be substantial
latitude in these compositions depending on what one
desires to achieve in ultimate magnetic properties.
Moreover, certain amounts of other rare earth metals
may be substituted for neodymium which will be
10 described hereinafter.

Example 12

Figure 16 shows demagnetization curves for
melt-spun $Nd_{0.33}(Fe_{0.95}B_{0.05})_{0.67}$ as a function of
temperature. The samples were remagnetized in the
15 pulsed 45 kOe field between temperature changes.
Elevated temperatures have some adverse effect on the
remanent magnetization of these materials. Experi-
mental evidence indicates that approxiately 40
percent of the H_{ci} may be lost between temperatures
20 of 400 and 500° C. This is generally comparable to
the losses experienced by mischmetal-samarium-cobalt,
and $SmCo_5$ magnets at like temperatures. Given the
high initial H_{ci} of my alloys, however, in many
applications such losses may be tolerated.

25 ### Example 13

Figure 17 shows demagnetization curves for
melt-spun $Nd_{0.15}(Fe_{0.95}B_{0.05})_{0.85}$ as a function of
temperature. When compared to Figure 10, it is clear
that higher atomic percentages of iron tend to improve
30 the magnetic remanence and, hence, energy product of
the subject alloys at elevated temperatures.

Example 14

Figure 18 shows a normalized plot of the log
of intrinsic coercivity as a function of temperature
35

for three different neodymium-iron-boron alloys. In
the higher iron content alloy, intrinsic coercivity
decreases less rapidly as a function of temperature
than in the higher neodymium fraction containing
5 compounds.

Example 15

Figure 19 shows the value of magnetic
remanence as a function of temperature in degrees
Kelvin for $Nd_{1-x}(Fe_{0.95}B_{0.05})_x$ alloys where
10 X = 0.85, 0.80, 0.67 and for $Nd_{0.4}(Fe_{0.97}B_{0.03})_{0.6}$.
Again, the higher iron content alloys show higher
remanence at elevated temperatures.

Example 16

Figure 20 shows magnetization dependence of
15 melt spun $Nd_{0.25}(Fe_{1-y}B_y)_{0.75}$ on temperature. The
higher boron content alloys showed a dip in the
magnetization curve at temperatures between about 100
and 300° Kelvin. The reason for this apparent
anomaly is not currently understood. The Curie
20 temperature (T_c) was substantially elevated by the
addition of boron: T_c = 453° K for no boron and
533° K with 3.75 atomic percent boron (Y = 0.05).
Figure 20 shows the effect of adding boron on Curie
temperature for several neodymium-iron-boron alloys.

25 ### Example 17

Figure 21 shows the effect of varying the
amount of neodymium in a neodymium-iron-boron alloy
on magnetization of melt-spun samples at temperatures
between 0 and 600° K. The dip between 100 and 300°
30 Kelvin is noted in all of the curves although the
high iron content alloy magnetization curve is
substantially flatter in that temperature range than
the higher neodymium content alloys.

35

29

Example 18

Figure 22 shows x-ray spectra (CuK alpha) of $Nd_{0.15}(Fe_{1-y}B_y)_{0.85}$, Y = 0.00, 0.03, 0.05, 0.07, 0.09 alloy samples ejected from 675 micron orifice
5   onto a quench wheel moving at V_s = 15 m/s. The selected samples exhibited maximum intrinsic coercivity for each boron level. The data X-ray were taken from finely powdered specimens over a period of several hours. The x-ray intensity units are on an
10   arbitrary scale.

The boron-free alloy X-ray spectra include Bragg reflections corresponding to the neodymium and Nd_2Fe_{17} phases, neither of which is believed to account for even a limited amount of coercivity in
15   these alloys since the highest Curie temperature of either (Nd_2Fe_{17}) is only 331° K. X-ray data indicate that the inclusion of boron in $[Nd_{0.15}(Fe_{1-y}B_y)_{0.85}]$, where $0.03 \lesssim y \lesssim 0.05$, stabilizes a Nd-Fe-B intermetallic phase. This phase is believed to be
20   responsible for the permanent magnetic properties. Its Curie temperature is well above that of any other known Nd-Fe compounds.

Example 19

Figure 23 compares the x-ray spectra of the
25   quenched surface of an $Nd_{0.25}(Fe_{0.95}B_{0.05})_{0.75}$ alloy ribbon to the free surface. The quenched surface is defined as that surface of the ribbon which impinges on the cooling substrate. The free surface is the opposite flat side of the ribbon which does not
30   contact the cooling substrate. Clearly, the free surface sample shows more crystallinity than the quenched surface. This may be explained by the fact that the free surface cools relatively slower than the quenched surface allowing more time for
35   crystallographic ordering of the elements.

30

Example 20

Figure 24 displays differential scanning calorimetry data for optimum directly quenched $Nd_{0.25}(Fe_{1-y}B_y)_{.75}$ which alloys exhibit
5 maximum coercivity from Figure 2. The data were taken ata heating rate of 80° K per minute. The addition of boron clearly increases the crystalline character and reduces the amorphous or glass-like characteristics of these optimum melt spun alloys.
10 This was not expected as boron is known to promote glass formation in some other compositions, e.g. (Fe_8B_2). The Y = 0.05 alloys appear to have a particularly crystalline nature as indicated by the absence of any increased apparent specific heat (ASH)
15 release up to 1000° K. The sharp elevation in ASH at 940° K is believed to be associated with partial melting of the alloy.

Example 21

Figure 25 displays differential scanning
20 calorimetry data for $Nd_{0.15}(Fe_{1-y}B_y)_{0.85}$ alloys (y = 0.0, 0.05 and 0.09) quenched at V_s = 15 m/s and 30 m/s. X-ray data for the 15 m/s alloys are shown in Figure 16. The DSC tracings of all of the V_s = 15 m/s alloys, which are close to the optimum
25 quench, are relatively flat, confirming the pre-dominantly crystalline charater indicated by the X-ray data. In contrast, all of the V_s = 30 m/s alloys for y = 0.05 and 0.09 exhibit large increases in apparent specific heat in the vicinity of 850 -
30 900°K, indicating that randomly arranged atoms in the alloys undergo crystallization in the temperature range. X-ray patterns of the alloy before heating also indicate glass-like or amorphous behavior, exhibiting a single broad peak centered at 20 - 40°.
35

31

In contrast, the DSC and X-ray data for the
$y = 0.0$ (boron-free) alloy was little changed between
$V_s = 15$ and 30 m/s. Moreover, no large increase in
apparent specific heat occurred above 900°K. Boron
5 is necessary to achieve a microstructure in an
overquenched alloy which can be later annealed to a
magnetically hard state. Without boron, one cannot
anneal an overquenched alloy to a magnetically hard
state. This is because the Nd-Fe-B phase is not
10 present.

Example 22

Figure 26 shows typical demagnetization
curves for various permanent magnet materials and
lists values for their maximum energy products.
15 Clearly, only $SmCo_5$ shows slightly better room
temperature magnetic properties than the subject
neodymium-iron-boron compositions. Bonded $SmCo_5$
powder magnets are substantially weaker. It is
believed that the subject RE-TM-B compositions could
20 be used in high quality, high coercivity, hard magnet
applications at substantially less cost than oriented
$SmCo_5$ magnets both because of the lower cost of the
constituent elements and easier processing. The
subject hard magnet compositions have much better
25 properties than conventional manganese-aluminum-
carbon, Alnico, and ferrite magnets.

Example 23

Figure 27 shows that adding boron to
$ND_{1-x}(Fe_{1-y}B_y)_x$ alloys substantially elevates the
30 alloys' apparent Curie temperatures. So far as
practical application of the subject invention is
concerned, increased Curie temperature greatly
expands the possible uses for these improved hard
magnet materials. For example, magnets with Curie
35

32

temperatures above about 500°K (237° C) could be used
in automotive underhood applications where temperatures
of 150° C may be encountered.

5   The data points which are blacked-in in
Figure 27 particularly show the substantial increase
in Curie temperature provided by adding 5 percent
boron based on the iron content of the neodymium-iron
melt spun alloys having less than 40 atomic percent
neodymium. Like alloys without boron showed a marked
10 tendency to lowered apparent Curie temperature. That
is, including boron not only elevates Curie tempera-
ture but does so at relatively lower rare earth
concentrations. Thus, adding boron to suitable RE-TM
alloys increases intrinsic magnetic coercivity and
15 Curie temperature at relatively high iron concentra-
tions. These results are very desirable.

Example 24

    Experiments were conducted on iron-rich
alloys to determine whether comparable hard magnet
20 characteristics could be induced in the subject
RE-TM-B compositions by annealing magnetically soft
substantially amorphous forms of the alloy. Refer-
ring to Figure 28, a representative alloy of
$Nd_{0.15}(Fe_{0.95}B_{0.05})_{0.85}$ was melt-spun onto a chill
25 disc having a surface velocity V_s of 30 meters per
second. The ribbon so produced was amorphous and had
soft magnet characteristics indicated by the sharp
slope of its demagnetization curve (no anneal, V_s =
30 m/s, line in Figure 28). When this ribbon was
30 annealed at about 850°K for about 15 minutes the
maximum magnetic coercivity increased to about 10.5
kOe and the alloy exhibited hard magnetic character-
istics.

35

33

When a like Nd-Fe-B alloy was melt-spun and quenched in like manner on a chill disc having a surface velocity of V_s = 15 meters per second, an amorphous to finely crystalline alloy was produced with an intrinsic room temperature coercivity of about 17 kOe (no anneal, V_s = 15 m/s, line in Figue 28), much higher than that of the alloy quenched at V_s = 30 either before or after annealing. When the alloy melt spun at V_s = 15 meters per second was annealed at about 850° K, its intrinsic coercivity dropped to levels nearly matching those of the annealed V_s = 30 samples.

Example 25

An alloy of $Nd_{0.14}(Fe_{0.95}B_{0.05})_{0.86}$ was prepared by ejecting a 25 gram sample of molten alloy from a quartz crucible onto the perimeter of a chromium plated copper disc rotating at a speed V_s = 30 meters per second. The orifice size was approximately 670 micron meters and the ejection pressure was approximately 3.0 psi argon. This produced overquenched alloys with virtually no hard magnetic properties. The line marked "no anneal" on Figure 29 shows the coercivity and remanence of the alloy as melt spun.

The melt spun ribbon was coarsely crushed and samples weighing approximately 60 milligrams each were weighed out. The subsequent heating or annealing regimen was carried out under one atmosphere of flowing argon in a Perkin-Elmer (DSC-ii) differential scanning calorimeter. The calorimeter was initially at room temperature with the temperature being raised at a rate of 160° K per minute up to a peak temperature of 950° K. The samples were cooled to room temperature at the same rate. The demagnetization data were

34

taken on a magnetometer after first magnetizing the
samples in the pulsed field of about 40 kiloGauss.

Figure 29 shows second quadrant demagnet-
ization curves for the samples as a function of how

5   long they were maintained at the peak anneal tempera-
ture of 950° K. The line marked 0 min. represents
the magnetic characteristics of a sample elevated to
950°K at the ramp rate of 160° K per minute and then
immediately cooled to room temperature at the same

10   rate of 160°K per minute. The curves for 5, 10 and
30 minutes refer to maintaining the samples at the
950° K peak temperature for periods of 5, 10 and 30
minutes at heating and cooling ramp rates of 160°K
per minute.

15   It is clear from this data that holding a
sample at an elevated temperature of 950°C for any
substantial period of time adversely affects the
magnetic strength of the annealed alloy. As the best
magnetic properties were obtained for the samples

20   which were rapidly annealed and then rapidly cooled,
it appears that the speed of the annealing process is
significant to the formation of the desired hard
magnetic properties in the alloys. While a rapid
convection heating is effective in creating the

25   permanent magnetic phase in the rare earth-iron-boron
alloys, other processes such as mechanically working
or hot pressing overquenched alloys could also
promote the formation of the very finely crystalline
permanent magnetic phase.

30   ## Example 26

A $Nd_{0.14}(Fe_{0.95}B_{0.05})_{0.86}$ alloy was
melt spun at quench wheel speeds V_s = 27.5 and 30
m/s. The samples were annealed in a differential
scanning calorimeter at heating and cooling ramp

35

rates of 40 and 160°K per minute. The alloy quenched at V_s = 27.5 m/s exhibited higher remanence than the V_s = 30.0 m/s alloy. For both values of V_s, the sample annealed at the higher ramp rate of 160°K

5   per minute showed higher second quadrant remanence and coercivity than those annealed at the 40°K per minute ramp rate. Thus, rapid heating and low time at maximum temperature appear to promote formation of crystallites in the desired size range between about

10 20 and 200 nanometers. Over-annealing probably causes excess crystal growth and the creation of larger than optimum single domain sized particles. Excessive crystal growth, such as that brought about by extended anneal (see Figure 29, e.g.) tends to

15 degrade magnetic strength.

Example 27

Figure 31 shows a plot of maximum energy product for $Nd_{0.14}(Fe_{0.95}B_{0.05})_{0.86}$ alloy. The circular open data points represent energy products

20 for alloy directly quenched at the quench wheel speeds V_s indicated on the X axis. The other data points represent the maximum energy product for alloy quenched at the V_s indicated on the X-axis and then annealed in a differential scanning calorimeter at a

25 heating and cooling ramp rate of 160°K per minute to maximum temperatures of 1000, 975 and 950°K.

A maximum energy product of 14.1 megaGauss Oersted was reached for the alloy directly quenched at an approximate wheel speed of 19 m/s. The alloy

30 directly quenched at wheel speeds greater than about 20.5 meters per second shows rapidly decreasing energy product with quench wheel speed. At about V_s = 30 meters per second, the alloy as quenched has substantially no energy product. The solid

35

round, triangular and square data points represent the measured maximum energy products for the alloy quenched at the corresponding V_s on the X axis after they have been annealed to maximum temperatures

5 of 1000, 975 and 950°K, respectively. The annealing steps were conducted in a differential scanning calorimeter at a heating and cooling ramp rate of 160°K per minute. It is evident from Figure 31, that the alloy can be overquenched and then annealed back

10 to produce a form of the alloy with high magnetic energy product. This is a strong support for the hypothesis that the phase responsible for the permanent magnetic properties in the alloy is finely crystalline and is probably commensurate with optimum

15 single domain size. The overquenched alloy, i.e., in this case those melt spun ribbons quenched at a wheel speed greater than about 20 meters per second would either be completely amorphous or have crystallites or particle sizes in their microstructures smaller

20 than optimum single magnetic domain size. The heating step is believed to promote the growth of the crystallites or particles within the microstructure to achieve the near optimum single domain size. Surprisingly, the size of the crystallites after a

25 rapid heating to 950°K is fairly uniform throughout the ribbon thickness.

Figure 32 shows the second quadrant magnetization curves for the alloy of Figure 31 as directly quenched at the indicated wheel speeds. Figure 33

30 shows X-ray diffraction patterns for an ingot of the alloy and for the alloy as it comes off the quench wheel at the indicated wheel speeds. It is apparent from these X-ray spectra that increasing the wheel speed decreases the occurrence of specific peaks and

35

creates a much more amorphous looking pattern. The
pattern for V_s = 35 m/s is characteristic of an
amorphous, glassy substance. Annealing any of the
alloys in accordance with the regiment described with
5   respect to Figure 31 creates an X-ray diffraction
pattern similar to that for V_s = 19 m/s of Figure
33. However, much better magnetic properties are
observed for suitably annealed samples which
initially show some incipient crystallization like
10 V_s = 21.7 m/s in Figure 33. Annealing amorphous
alloy with a glassy X-ray pattern (e.g. V_s = 35 or
40 m/s) creates permanent magnetic properties but the
remanence is lower.

A comparison was made between the second
15 quadrant magnetic characteristics of the
$Nd_{0.14}(Fe_{0.95}B_{0.05})_{0.86}$ alloy originally quenched
at wheel speeds of 20.5 m/s (Figure 35) to alloy
quench at wheel speeds of 35 m/s (Figure 36). The
slightly overquenched material (V_s = 20.5 m/s)
20 showed magnetic remanence over 8 kiloGauss and
coercivity over 12 kiloOersteds and a maximum energy
product of 13.7 megaGauss Oersted. On the other
hand, the grossly overquenched alloy (V_s = 35 m/s)
showed maximum magnetic remanence below 8 megaGauss
25 Oersted. The maximum energy product for the greatly
overquenched V_s = 35 m/s alloy was 11.9 megaGauss
Oersted.

Figure 34 shows differential scanning
calorimeter traces for the alloys of Figure 31
30 quenched at wheel speed V_s = 19, 20.5 and 35 m/s.
That quenched at 19 meters per second representing
the optimum direct quenched alloy shows a decrease in
apparent specific heat (ASH) at about 575°K and then
a slight increase in ASH up to the maximum operating
35

38

temperature available of the DSC ($\sim$ 1000°K). The
alloy that was overquenched slightly at a V_s = 20.5
m/s also showed a decrease in ASH at 575°K but it
also exhibits a sustantial increase in ASH at about
5   875°K. It has been theorized that this peak at 875°K
is associated with crystallization and growth of the
magnetic phase in the alloy. The substantially
amorphous, grossly overquenched alloy melt spun at
V_s = 35 m/s does not exhibit a decrease in ASH at
10   575°K but shows an even larger increase in ASH at
about 875°K.

In this and other examples, $RE_{1-x}(Fe_{1-y}B_y)_x$
where 0.88 $\lesssim$ x $\lesssim$ 0.86 and 0.05 $\lesssim$ y $\lesssim$ 0.07 is
believed to be the nominal composition of the phase
15   primarily responsible for the hard magnetic proper-
ties. The preferred RE elements are neodymium and
praseodymium which are virtually interchangeable with
one another. The phase, however, is relatively
insensitive to the substitution of as much as 40
20   percent of other rare earth elements for Pr and Nd
without its destruction. In the same vein, substan-
tial amounts of other transition metals can be
substituted for iron without destroying the phase.
This phase is believed to be present in all composi-
25   tions of suitable microstructure having hard magnetic
properties. Varying the amounts of the constituents,
however, changes the amount of the magnetic phase
present and consequently the magnetic properties,
particularly remanence.
30   Figure 37 is a scanning electron micrograph
of the fracture surface of an overquenched (V_s = 30
m/s) $Nd_{0.14}(Fe_{0.95}B_{0.05})_{0.86}$ ribbon showing the
microstructure, near the free surface, the middle and
the quench surface. The slower cooling free surface
35

38

shows a very slight degree of crystallization which
shows up on the micrograph as a speckled appearance.
The dot in the middle frame of the Figure is an
extraneous, nonsignificant SEM feature. The middle

5   and quench surfaces of the ribbon appear to be
substantially amorphous, that is, discrete crystal-
lites are not obviously distinguishable.

        Figure 38 is an SEM of the fracture
surface of the overquenched (V_s = 30 m/s)

10    $Nd_{0.14}(Fe_{0.95}B_{0.05})_{0.86}$ alloy after a DSC anneal
to a maximum temperature of 950°K at a heating and
cooling ramp rate of 160°K per minute. It is clear
from this SEM that fairly regularly shaped crystal-
lites or particles have formed in the ribbon as a

15   result of the annealing step. These crystallites
have an average size between 20 and 400 nanometers
but are not as uniformly sized throughout the
thickness of the ribbon as the crystallites of the
14.1 MG·Oe directly quenched alloy. A uniform

20   crystallite size seems to be characteristic of the
highest energy product alloys. The measured pre-
ferred size range for these crystallites is in the
range from about 20 to 400 nanometers, preferably
about 40 - 50 nanometers average.

25   Figure 39 shows the second quadrant magnet-
ization curves for optimally directly quenched alloys
of this example compared with the overquenched and
annealed V_s = 20.5 and 35 m/s samples.

Example 28

30   Figure 11 is a plot of magnetic remanence
of $Nd_{0.15}(Fe_{1-x}B_y)_{0.85}$ for boron-free and y = 0.03,
0.05, 0.07, 0.09 alloys. The samples were cast from
an orifice approximately 675 microns in size at a
quench rate of approximately 27.5 meters per second.

35

As will be described hereinafter, the samples were
heated to a peak temperature of approximately 975°K
in a differential scanning calorimeter at a heating
and cooling ramp rate of approximately 160°K per
5   minute. The boron-free alloy y = 0.0 showed substan-
tially no coercivity after anneal and magnetization.
That containing 0.03 boron exhibited a coercivity of
approximately 6 kiloOersteds. At a boron content of
0.05 both magnetic remanence and   coercivity were
10   substantially increased to approximately 17.5 kilo-
Oersted and 7.5 kiloGauss, respectively. At a boron
content of 0.07, the coercivity increased while the
magnetic remanence droped slightly. At a boron
content of 0.09, both remanence and coercivity
15   dropped with respect to the 0.07 boron content.

Example 29

Figure 40 is a demagnetization plot for
$Pr_{0.135}(Fe_{0.935}B_{0.065})_{0.865}$ alloy that was melt spun
through a 675 micron orifice onto a quench wheel
20   moving at V_s = 30 m/s. The resultant alloy ribbon
was overquenched and had substantially no magnetic
coercivity. Samples of the ribbon were annealed in a
differential scanning calorimeter at a heating and
cooling ramp rate of 160°K per minute to maximum peak
25   temperatures of 900, 925 and 975°K. The alloy
heated to the 900°K maximum temperature had the
highest magnetic remanence. Increasing the peak
anneal temperature tended to reduce the remanence
slightly but very much increased the coercivity.

30   Clearly, praseodymium is also useful as the
primary rare earth constituent of rare earth-iron-
boron hard magnetic phase. It also appears to be
evident that control of the time and temperature of
annealing overquenched originally not permanently

35

magnetic alloy can be controlled in such manner as to tailor the permanent magnetic properties. It seems that a rapid higher temperature anneal while reducing the remanence somewhat can be used to achieve very

5   high magnetic coercivities. On the other hand, using lower temperature rapid anneals may tend to maximize the energy product by increasing the magnetic remanence still at coercivities greater than 15 kiloOersted.

10   Example 30

Figure 41 shows demagnetization curves for $RE_{0.135}(Fe_{0.935}B_{0.065})_{0.865}$ alloy where RE is praseodymium, neodymium, samarium, lanthanum, cerium, terbium or dysprosium. In each alloy, only a single

15   rare earth was used, i.e., the rare earths were not blended with one another to form an alloy sample. Each alloy sample was melt spun through an ejection orifice approximately 675 microns in size onto a quench wheel rotating at V_s = 30 m/s. Each of the

20   alloys as formed had less than one kiloOersted coercivity and was overquenched. The alloy samples were annealed in the differential scanning calorimeter at heating and cooling ramp rates of 160°K per minute to a maximum temerature of 950°K.

25   Praseodymium and neodymium were the only sole rare earth elements of those tried which created annealed alloys with high coercivity remanence and energy products. Samarium and lanthanum showed very slight coercivities coupled with fairly steep

30   remanence curves. The cerium showed some coercivity and remanence. Terbium exhibited low coercivity and very low remanence. While none but the pure praseodymium and neodymium alloys showed characteristics suitable for making very strong permanent

35

42

magnets, the hysteresis characteristics of the other
rare earths may provide magnetic materials which
could be very useful for soft magnetic or other
magnetic applications.

5   Example 31
        Figure 42 shows the effect of substituting
20 percent of a different rare earth based on the
amount of neodymium and such rare earth in
$(Nd_{0.8}RE_{0.2})_{0.135}(Fe_{0.935}B_{0.065})_{0.865}$ alloys. Each
10   of these 80 percent neodymium and 20 percent other
rare earth alloys was melt spun and processed as in
Example 30. The substitution of 20 percent
dysprosium, praseodymium and lanthanum created alloys
with good permanent magnetic properties. The terbium
15   containing alloy had a coercivity higher than could
be measured by the magnetometer. The samarium
containing alloy exhibited a remanence over 8
kiloGauss and a coercivity of about 6 kiloOersted.
Table 1 shows the compositions, intrinsic
20   coercivities, magnetic remanence and energy product
for the alloys shown in Examples 31 and 32.

25

30

35

42

Table I

Composition	H_{ci} (kOe)	B_r (kG)	$(BH)_{max}$
$La_{0.135}(Fe_{0.935}B_{0.065})_{0.865}$	0	0	0
$(Nd_{0.8}La_{0.2})_{0.135}(Fe_{0.935}B_{0.065})_{0.865}$	11.6	7.8	12.1
$Ce_{0.135}(Fe_{0.935}B_{0.065})_{0.865}$	2.2	3.4	1.3
$(Nd_{0.8}Ce_{0.2})_{0.135}(Fe_{0.935}B_{0.065})_{0.865}$	13.0	7.5	11.0
$(Nd_{0.95}Ce_{0.05})_{0.135}(Fe_{0.935}B_{0.065})_{0.865}$	12.3	7.8	11.2
$Pr_{0.135}(Fe_{0.935}B_{0.065})_{0.865}$	16.8	7.7	12.4
$(Nd_{.8}Pr_{.2})_{0.135}(Fe_{0.935}B_{0.065})_{0.865}$	15.7	7.7	11.9
$Sm_{0.135}(Fe_{0.935}B_{0.065})_{0.865}$	1.8	6.0	2.6
$(Nd_{.8}Sm_{.2})_{0.135}(Fe_{0.935}B_{0.065})_{0.865}$	5.7	8.3	9.82
$Tb_{0.135}(Fe_{0.935}B_{0.065})_{0.865}$	1.2	0.3	0.1
$(Nd_{.8}Tb_{.2})_{0.135}(Fe_{0.935}B_{0.065})_{0.865}$	>20	6.7	9.8
$(Nd_{.95}Tb_{0.05})_{0.135}(Fe_{0.935}B_{0.065})_{0.865}$	15.8	7.7	11.6
$Dy_{0.135}(Fe_{0.935}B_{0.065})_{0.865}$	1.5	0.3	0.1
$(Nd_{.8}Dy_{.2})_{0.135}(Fe_{0.935}B_{0.065})_{0.865}$	18.3	6.8	9.90

It is clear from this data that substantial amounts of rare earth elements other than neodymium and praseodymium can be incorporated in rare earth-iron-boron alloys to create very finely crystalline permanent magnetic alloys. Neodymium and praseodymium metals can be mixed in suitable proportions with other rare earth elements to tailor the second quadrant magnetic characteristics for a particular application. For example, if a very high coercivity permanent magnet were desired terbium could be added to the composition. On the other hand, if magnetic remanence were the desired characteristic, it may be advantageous to add samarium.

44

Example 32

Figure 43 shows the demagnetization curves for $Nd_{0.135}(TM_{0.935}B_{0.065})_{0.865}$ where TM are the transition metals iron, cobalt and nickel. In this
5   Figure, the transition metals were not mixed with one another to form the alloy. The alloys were melt spun and processed as in Example 30.

Of the transition metal elements, only iron yields an alloy with very good permanent magnetic
10 properties. The cobalt shows moderate intrinsic coercivities and remanence, while the nickel containing alloy shows high coercivity but practically no magnetic remanence.

Figure 44 shows the effect of adding 10
15 percent transition metal based on the amount of iron in the alloy to alloys of

$Nd_{0.135}(Fe_{0.841}TM_{0.094}B_{0.065})_{0.865}$.   Figure 45 shows like curves for the addition of 20 percent based on the atomic percent of iron for alloys of
20 $Nd_{0.135}(Fe_{0.748}TM_{0.187}B_{0.065})_{0.86}$.   These alloys were also processed as in Example 30.

The substitution of 20 percent cobalt for iron in the alloys does not seem to have any deleterious affect, although 100 percent cobalt containing
25 alloy does not exhibit very high remanence and coercivity. The incorporation of nickel, chromium and manganese seem to substantially dilute the hard magnetic properties of the pure iron alloy. The addition of copper radically lowers the coercivity
30 and somewhat lowers the magnetic remanence. At alloy addition levels of 20 percent based on the iron content, nickel and chromium very much reduced the coercivity and the remanence as compared to the all iron alloys. Manganese produces an alloy with no
35 second quadrant coercivity or remanence.

44

45

Table II shows the intrinsic coercivity, magnetic remanence and energy product for neodymium transition metal boron alloys. The reported values are for the best overall combination of coercivity remanence and energy product where the aim is to produce a permanent magnet. Generally, such data represent the squarest shaped second quadrant demagnetization curve.

Table II

Composition	H_{ci} (kOe)	B_r (kG)	$(BH)_{max}$
$Nd_{0.135}(Fe_{0.748}Cr_{0.187}B_{0.065})_{0.865}$	3.7	3.0	1.0
$Nd_{0.135}(Fe_{0.841}Cr_{0.094}B_{0.065})_{0.865}$	12.0	5.1	5.42
$Nd_{0.135}(Fe_{0.888}Cr_{0.047}B_{0.065})_{0.865}$	15.1	6.4	8.25
$Nd_{0.135}(Fe_{0.912}Cr_{0.023}B_{0.065})_{0.865}$	13.4	7.4	11.4
$Nd_{0.135}(Fe_{0.748}Mn_{0.187}B_{0.065})_{0.865}$	0	0	0
$Nd_{0.135}(Fe_{0.841}Mn_{0.094}B_{0.065})_{0.865}$	9.0	4.5	4.1
$Nd_{0.135}(Co_{0.935}B_{0.065})_{0.865}$	1.3	3.0	0.6
$Nd_{0.135}(Fe_{0.748}Co_{0.187}B_{0.065})_{0.865}$	14.5	7.90	12.9
$Nd_{0.135}(Fe_{0,841}Co_{0.094}B_{0.065})_{0.865}$	13.7	7.95	12.7
$Nd_{0.135}(Ni_{0.935}B_{0.065})_{0.865}$	15	0.15	0.1
$Nd_{0.135}(Fe_{0.748}Ni_{0.187}B_{0.065})_{0.865}$	4.7	5.2	4.0
$Nd_{0.135}(Fe_{.841}Ni_{0.94}B_{0.065})_{0.865}$	11.7	7.2	10.2
$Nd_{0.135}(Fe_{0.912}Ni_{0.023}B_{0.065})_{0.865}$	13.0	7.8	12.0

It appears from these data that cobalt is interchangeable with iron at levels up to about 40 percent in the subject alloys. Chromium, manganese and nickel degrade the hard magnetic properties of the alloys.

46

Small amounts of the elements zironium and titanium were added to neodymium-iron-boron alloys, as set forth in Table III. The alloy compositions were melt spun and processed as in Example 30. The

5 inclusion of small amounts (about 1½ atomic percent) of these elements still produced good hard magnetic alloys. The addition of zirconium had a tendency to substantially increase the intrinsic magnetic coercivity of the base alloy.

10
Table III

Composition	H_{ci} (kOe)	B_r (kG)	$(BH)_{max}$
$Nd_{0.135}(Fe_{0.916}Zr_{0.019}B_{0.065})_{0.865}$	18.5	7.25	10.9
$Nd_{0.135}(Fe_{0.916}Ti_{0.019}B_{0.065})_{0.865}$	16.5	7.25	10.3

15

Example 33
Substitutions for boron in
$Nd_{0.135}(Fe_{0.935}B_{0.065})_{0.865}$ alloys were made.

20 The substitute elements included carbon, aluminum, silicon, phosphorus and germanium as set forth in Table IV. The alloys were melt spun and processed as in Example 30 above. For all but the carbon, the resultant alloys had no magnetic energy product.

25 Only carbon showed a slight energy product of 0.9 megaGauss with low values of intrinsic coercivity and remanence.

Table IV

30

Composition	H_{ci} (kOe)	B_r (kG)	$(BH)_{max}$
$Nd_{0.135}(Fe_{0.935}C_{0.065})_{0.865}$	.75	2.25	.9
$Nd_{0.135}(Fe_{0.935}Al_{0.065})_{0.865}$	0	0	0
$Nd_{0.135}(Fe_{0.935}Si_{0.065})_{0.865}$	0	0	0
$Nd_{0.135}(Fe_{0.935}P_{0.065})_{0.865}$	0	0	0
$Nd_{0.135}(Fe_{0.935}Ge_{0.065})_{0.865}$	.2	0.1	0

35

The preceding Examples set out preferred embodiments of the subject invention. The combined permanent magnetic properties of coercivity, remanence and energy product for the subject RE-Fe-B alloys are

5   comparable to those heretofore achieved only with oriented $SmCo_5$ and Sm_2Co_{17} magnets. Not only are Pr, Nd and Fe less expensive than samarium and cobalt, but the subject magnetic alloys are easier and less expensive to process into permanent magnets.

10 Compilation of data from the several Examples indicates that the compositional range over which a major phase with the exhibited magnetic properties forms is fairly wide. For $Re_{1-x}(Fe_{1-y}B_y)_x$ alloys, X is preferably in the range of from about

15 0.5 to 0.9 and y is in the range of from about 0.005 to 0.1. The balance of the alloys is preferably iron. Up to about 40 percent of the iron can be replaced with cobalt with no significant loss of magnetics. Neodymium and praseodymium appear to be

20 fairly intechangeable as the principal rare earth constituent. Other rare earth elements such as samarium, lanthanum, cerium, terbium and dysprosium, probably in amounts up to about 40 percent of the total rare earth content, can be incorporated with

25 neodymium and/or praseodymium without destruction of the crystal structure of the magnetic phase or substantial loss of permanent magnetism. These rare earths can be added to purposefully modify the demagnetization curves.

30 In view of the experimental data, the near optimum Nd-Fe-B and Pr-Fe-B alloy nominal composi-tions for maximizing permanent magnetic properties are approximately $RE_{0.135}(Fe_{0.935}B_{0.065})_{0.865}$ or expressed in terms of atomic fractions of the

35 three constituent elements, $RE_{0.135}Fe_{0.809}B_{0.056}$

48

or in terms of atomic fractions normalized to boron, $RE_{2.4}Fe_{14.4}B_1$. The subject samples were prepared from commercially available constituents which do contain some residual contaminants such as oxides,

5 nitrides, etc. Should higher purity constituents be employed, the composition, specifically the Nd to combined Fe-B ratio, would probably change slightly.

The SEM data for the highest energy product direct quenched alloys indicate that the crystallites

10 or particles within the microstructure have a fairly regular shape. Magnetic data also suggest that the crystal structure of the stable Nd-Fe-B intermetallic phase has high symmetry. Evidence for this is the high ratio of remanent to saturation magnetization.

15 Electron microprobe analysis and TEM data suggest the presence of a small amount of a second phase of unidentified composition which may also contribute to the magnetic properties.

The directly quenched and overquenched and

20 annealed alloy ribbons appear to be magnetically isotropic as formed. This is evidenced by the fact that the ribbon can be magnetized and demagnetized to the same strength in any direction. However, if single optimum magnetic domain size powder particles

25 or the crystallites themselves can be caused to orient along a crystallographically preferred magnetic axis, it is possible that highly magnetically aniso- tropic alloys having much higher magnetic energy products than are reported herein would result.

30 In order to characterize the stable magnetic phase, the initial X-ray diffraction data were studied and neutron diffraction data were obtained. As seen in Figure 33, the X-ray diffraction data for melt-spun ribbon having optimum magnetic energy

35 products have peaks which are broadened counterparts

49

of those in the pattern from a single phase starting
ingot with long range crystallographic ordering.
Therefore, the Cu k-alpha d-spacing patterns for
ingot alloy were used to determine the crystal
5 structure of the major magnetic phase. X-ray
patterns strongly suggested a tetragonal crystal
structure with room temperature lattice constants of
a = 8.78 angstroms and c = 12.18 angstroms.

An effort was then made to investigate the
10 space groups of the apparently tetragonal crystallites
of the magnetic phase in accordance with the
International Tables for X-Ray Crystallography,
edited by N. Henry and K. Lonsdale (Kynoch,
Birmingham, 1952), Vol. 1. The space group $P4_2/mnm$
15 (#136) was chosen as the most probable choice because
it has a large number of atomic sites, several of
which have high occupancy.

To discover the positions of the neodymium
and most of the iron atoms in this $P4_2/mnm$ structure,
20 neutron diffraction data were taken of powdered
melt-spun alloy ribbon having the formula
$Nd_{0.135}(Fe_{0.935}B_{0.065})$ at 673°K. This temperature
is above the Curie temperature so that observed
scattering is due only to nuclear and not magnetic
25 scattering. A computer program based on that
developed by H.M. Rietveld, Journal of Applied
Crystallography, Vol. 2, No. 65 (1969) was used to
synthetically generate neutron diffraction data
assuming different atomic positions of the Nd, Fe and
30 B atoms.

35

Figure 46(a) displays observed neutron
diffraction data; Figure 46(b) shows the calculated
spectrum which best corresponds with the high
temperature neutron data; and Figure 46(c) shows the
difference between the observed and calculated data.
The goodness-of-fit index is 11.7 percent while the
statistical uncertainty is 8.8 percent. The formula
per unit cell associated with Figure 46(b) is
$Nd_8Fe_{56}B_4$ and the calculated density is 7.6
g/cm^3 which agrees with the measured density. This
would mean that the atomic formula for the major
phase of the magnetic alloys of this invention would
be $Nd_2Fe_{14}B_1$. The calculated data were
sensitive to both the number and position of the
boron atoms. Eight Nd atoms were found to occupy f
and g sites; 56 iron atoms to occupy k_1, k_2,
j_1, j_2, e and c sites; and 4 boron atoms to
occupy g sites. Table V summarizes the symmetry
sites and positions which generate the computed
pattern.

Table V

Atom	Occupany	Symmetry Position	Coordinates		
			x	y	z
Nd	4	f	0.273	0.273	0.0
Nd	4	g	0.128	-0.128	0.0
Fe	16	k_1	0.227	0.564	0.870
Fe	16	k_2	0.036	0.356	0.175
Fe	8	j_1	0.099	0.099	0.203
Fe	8	j_2	0.686	0.686	0.751
Fe	4	e	0.0	0.0	0.391
Fe	4	c	0.0	0.5	0.0
B	4	g	0.364	-0.364	0.0

Figure 47 shows the atomic arrangement of four unit cells in the basal plane, z = 0. Above this plane at z = 0.16 and 0.84 (in units of c) lie hexagonal puckered arrays of iron atoms (Figure 48).

5   Figure 49 shows the layers of iron atoms at locations z = 0.25 and 0.75. Figure 50 shows iron nets projected onto the z = 0.34 and 0.66 planes. Figure 51 shows the plane containing Nd, Fe and B atoms midway along the c axis at z - 0.5 Figure 52 shows a

10   view of one entire unit cell. The relative length of the c axis is exaggerated to emphasize the puckering of the hexagonal iron meshes. The preferred magnetic axis, i.e. that axis of alignment which yields the highest magnetic anisotropy, is the crystallographic

15   c axis.

Rapid solidification of the alloy is believed to create a condition wherein the individual crystallites or particles in the alloy microstructure are about the same size or smaller than optimum

20   single magnetic domain size. The optimum magnetic domain size is believed to about 40 - 50 nanometers average diameter. Alloys having crystallites in the size range of about 20 - 400 nanometers exhibit permanent magnetic properties. Alloys having smaller

25   crystallites (< 20 nanometers) may be heated to promote crystallite growth to optimum magnetic domain size.

The paths by which optimum crystallite size alloy can be made are (1) direct quench from the melt

30   by means of a controlled quench rate process such as melt spinning, or (2) overquench to a microstructure having smaller than optimum single domain size crystallites followed by a heating process to promote crystallite growth to near optimum single magnetic

35   domain size.

52

In summary, I have discovered new and
exceptionally strong magnetic alloys based on the
rare earth elements neodymium and praseodymium, the
transition metal element iron and a small amount of
5   the element boron. The inclusion of boron in the
RE-Fe systems provides many apparent advantages
including the creation of an equilibrium phase with
high apparent Curie temperature, a higher allowable
ratio of iron to the more expensive rare earth
10   constituents, a broad quench rate over which the
optimum finely crystalline microstructure magnetic
phase forms, and an ability to anneal overquenched
alloy to create the optimum finely crystalline
microstructure. The crystalline phase which forms is
15   also tolerant to the substitution of limited amounts
of many other constituents.

        It appears that the major phase of the
magnetic alloys has a tetragonal crystal structure
where the length of the a axis is about 8.78
20   angstroms and the c axis is about 12.18 angstroms.
The composition of this phase is $RE_2Fe_{14}B_1$ as
determined by neutron diffraction analysis. I have
also discovered efficient and economical means of
making the subject alloys in forms adapted for the
25   production of a new breed of permanent magnets. It
is expected that these magnets will find application
in many industrial environments.

        While my invention has been described in
terms of specific embodiments thereof, other forms
30   may be readily adapted by one skilled in the art.
Accordingly, the scope of my invention is to be
limited only by the following claims.

35

The embodiments of the invention in which an exclusive property or privilege is claimed are defined as follows:

1. An alloy for permanent magnets comprising about 0.5 to 10 atomic percent boron, at least about 10 atomic percent of one or more rare earth elements taken from the group consisting of neodymium and praseodymium, and the balance iron or mixtures of iron and cobalt where ratio of iron to cobalt is greater than 3:2, said alloy being further characterized by the presence of a predominant phase of crystallites of $RE_2TM_{14}B_1$.

2. The alloy of Claim 1 where the average diameter of the crystals of the predominant phase is less than 400 nanometers.

3. A permanent magnet alloy composition containing a tetragonal crystal phase $Nd_2Fe_{14}B_1$.

4. A permanent magnet alloy composition containing a tetragonal crystal phase $Pr_2Fe_{14}B_1$.

5. A permanent magnet alloy composition containing a tetragonal crystal phase $RE_2Fe_{14}B_1$ where RE is neodymium and/or praseodymium.

6. The permanent magnet alloy composition of Claim 5 where the length of the crystallographic c axis is about 12.18 angstroms and the length of the a axis is about 8.78 angstroms.

7. The permanent magnet alloy composition of Claim 5 where the crystallographic c axis is the preferred axis of magnetization.

8. A tetragonal crystal having the atomic formula $(RE_{1-a}RE^1_a)_2(FE_{1-b}TM_b)_{14}B_1$ where RE is neodymium and/or praseodymium; RE^1 is one or more rare earth elements taken from the group consisting of yttrium, lanthanum, cerium, samarium, europium, gadolinium, terbium, dysprosium, holmium, erbium, thulium, ytterbium and lutetium; and TM is one or more transition metal elements taken from the group consisting of cobalt, nickel, manganese, chromium and copper; and $0 \leq a \leq 0.4$ and $0 \leq b \leq 0.4$.

9. An alloy composition comprising a tetragonal crystal structure with the atomic formula $RE_2TM_{14}B_1$ wherein RE is one or more rare earth elements and wherein neodymium and/or praseodymium comprise at least about 60 percent of the total rare earth elements; and TM is one or more transition metal elements where iron comprises at least about 60 percent of the total transition metal elements.

Fig. 1

Fig. 2

Gowling & Henderson

$Nd_{0.15}(Fe_{1-Y}B_Y)_{0.85}$

	X
□	0.03
○	0.05
△	0.07
◇	0.09

H_{ci} (kOe)

V_s (m/s)

Fig. 3

$Nd_{1-X}(Fe_{0.95}B_{0.05})_X$

	X
◇	0.70
△	0.75
□	0.80
●	0.85
▽	0.90

H_{ci} (kOe)

V_s (m/s)

Fig. 4

Gowling & Henderson

$Nd_{1-x}(Fe_{0.95}B_{0.05})_x$

B_r (kG)

	x
◇	0.70
△	0.75
□	0.80
●	0.85
▽	0.90

V_s(m/s)

Fig. 5

$Nd_{0.25}(Fe_{0.95}B_{0.05})_{0.75}$

V = 2.5 m/s

V = 7.5 m/s

V = 10 m/s

V_s = 25 m/s

M (kG)

H (kOe)

Fig. 6

Gowling & Henderson

Fig. 7

Fig. 8

Fig. 9

$Pr_{0.4}(Fe_{0.95}B_{0.05})_{0.6}$ △

$Pr_{0.4}Fe_{0.6}$ ▲

$H_{ci}(kOe)$

$V_S (m/s)$

Fig. 10

$Nd_{0.15}(Fe_{1-y}B_y)_{0.85}$

$y = 0.05$

$y = 0.09$

$y = 0.07$

$y = 0.03$

$y = 0.0$

$M (KG)$

$H (KOe)$

Gowling & Henderson

Fig. 11

Fig. 12

Gowling & Henderson

Fig. 13

Fig. 14

$Nd_{1-x}(Fe_{0.95}B_{0.05})_x$

x = 0.866

x = 0.85

x = 0.8

x = 0.75

x = 0.9

Fig. 15

H (KOe)

M (KG)

Gowling & Henderson

Fig. 16

$Nd_{0.33}(Fe_{0.95}B_{0.05})_{0.67}$

295 K

346 K   396 K   451 K

M (kG)

H (kOe)

Fig. 17

$Nd_{0.15}(Fe_{0.95}B_{0.05})_{0.85}$

295 K

348 K   390 K   450 K

M (kG)

H (kOe)

Gowling & Henderson

Fig. 18

Fig. 19

Gowling & Henderson

Fig. 20

Fig. 21

Gowling & Henderson

Fig. 22

Gowling & Henderson

1319034
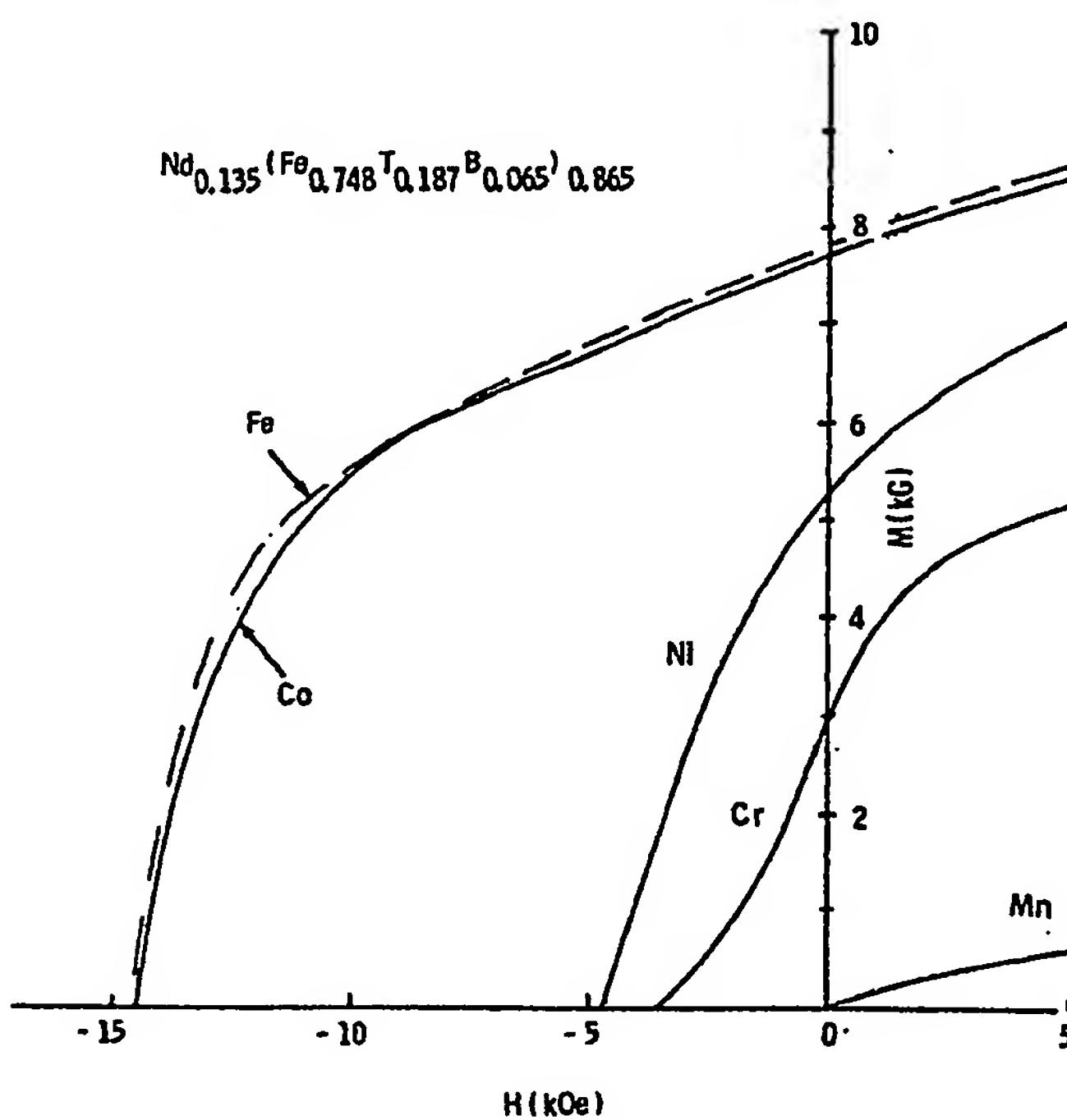
28-13

Fig. 23

Fig. 24

Gowling & Henderson

Fig. 25

Fig. 26

Gowling & Henderson

Fig. 27

$Nd_{1-x}(Fe_{1-y}B_y)_x$

Y=0.05

Y=0.0

$Nd_{0.15}(Fe_{0.95}B_{0.05})_{0.85}$

$V_S = 15m/s$ (NO ANNEAL)

$V_S = 15m/s$ (850 K)

$V_S = 30m/s$ (850 K)

$V_S = 30m/s$ (NO ANNEAL)

M(kG)

H (kOe)

Fig. 28

Gowling & Henderson

$Nd_{0.14}(Fe_{0.95}B_{0.05})_{0.86}$
$V_S = 30\ m/s$

0 min.

5 min.

10 min.

30 min.

NO ANNEAL

M (kG)

8

6

4

2

-15   -10   -5   0   5

H (kOe)

Fig.29

$Nd_{0.14}(Fe_{0.95}B_{0.05})_{0.86}$
$V_S = 27.5\ m/s$

$\alpha = 160\ K/min;\ 12.6\ MG\cdot Oe$
$\alpha = 40\ K/min;\ 11.4\ MG\cdot Oe$

$V_S = 30\ m/s$
$\alpha = 160\ K/min;\ 11.1\ MG\cdot Oe$
$\alpha = 40\ K/min;\ 10.4\ MG\cdot Oe$

10

8

6

4

2

M (kG)

-15   -10   -5   0   5

H (kOe)

Fig.30

Gowling & Henderson

Fig. 31

$$Nd_{0.135}(Fe_{0.946}B_{0.054})_{0.865}$$

$V_S = 19$ m/s
14.0 MG·Oe

$V_S = 20$ m/s
12.1 MG·Oe

$V_S = 20.5$ m/s
9.0 MG·Oe

$V_S = 21.7$ m/s
2.2 MG·Oe

$V_S = 35$ m/s
0.0 MG·Oe

$V_S = 27.5$ m/s
0.6 MG·Oe

H (KOe)

Fig. 32

Gowling & Henderson

(a)
$Nd_{0.135}(Fe_{0.945}B_{0.055})_{0.865}$
ingot

(b)
V_S = 19 m/s

(c)
V_S = 21.7 m/s

(d)
V_S = 35 m/s

X-RAY INTENSITY (arb. units)

20   30   40   50

2θ

Fig. 33

Gowling & Henderson

$Nd_{0.135}(Fe_{0.946}B_{0.054})_{0.865}$

(a)
$V_S = 19$ m/s

(b)
$V_S = 20.5$ m/s

(c)
$V_S = 35$ m/s

APPARENT SPECIFIC HEAT

400   600   800   1000

T (K)

Fig. 34

$Nd_{0.135}(Fe_{0.946}B_{0.054})_{0.865}$
$V_S = 20.5$ m/s

950 K
13.7 MG·Oe

975 K
13.3 MG·Oe

1000 K
12.9 MG·Oe

NO ANNEAL
9.0 MG·Oe

M (KG)

-15   -10   -5   0   5

H (KOe)

Fig. 35

Gowling & Henderson

$Nd_{0.135}(Fe_{0.946}B_{0.054})_{0.865}$
$V_S = 35\ m/s$

875 K
11.9 MG·Oe

1000 K
11.4 MG·Oe

950 K
11.2 MG·Oe

M (kG)

NO ANNEAL

875 K

H (kOe)

Fig. 36

$Nd_{0.135}(Fe_{0.935}B_{0.065})_{0.865}$

19 m/s

20.5 m/s

35 m/s

M (kg)

H (KOe)

Fig. 39

Fig. 37

Fig. 38

Free Surface

1 µm

Quench Surface

28.23

$Pr_{0.135}(Fe_{0.935}B_{0.065})_{0.865}$

975 K

900 K

925 K

M(kG)

H(kOe)

Fig. 40

$R_{0.135}(Fe_{0.935}B_{0.065})_{0.865}$

La

Pr

Sm

Ce

M(kG)

Nd

Tb, Dy

H(kOe)

Fig. 41

Gowling & Henderson

28.24

$(Nd_{0.8}R_{0.2})_{0.135}(Fe_{0.935}B_{0.065})_{0.865}$

Tb

Dy

Nd

La

Pr→

Ce

Sm

M (kG)

H (kOe)

Fig. 42

$Nd_{0.135}(T_{0.935}B_{0.065})_{0.865}$

Fe

Co

Ni

M (kG)

H (kOe)

Fig. 43

Gowling & Henderson

$Nd_{0.135}(Fe_{0.841}TM_{0.094}B_{0.065})_{0.865}$

Fig. 44

$Nd_{0.135}(Fe_{0.748}T_{0.187}B_{0.065})_{0.865}$

Fig. 45

Gowling & Henderson

(a) Observed

(b) Calculated

(c) Difference

INTENSITY

2θ

Fig. 46

Gowling & Henderson

⊕Nd f   ⊖Nd g   ●Fe c   ⊗B g

Fig. 47

⊕Fe k₁   ⊖Fe k₂   ⊕Fe j₁   ○Fe e

Fig. 48

⊕Fe j₂

Fig. 49

Gowling & Henderson

⊖ Fe k$_1$ ⊖ Fe k$_2$ ⊘ Fe j$_1$ ○ Fe e

Fig. 50

① Nd f   ⊖ Nd g   ● Fe c   ⊗ B g

Fig. 51

① Nd f   ⊖ Nd g

● Fe c   ○ Fe e   ⊘ Fe j$_1$ ○ Fe j$_2$ ⊘ Fe k$_1$ ○ Fe k$_2$ ○ B g

Fig. 52

Gowling & Henderson